Supplementary Information

High-Power Energy Storage and Stability of $Ti_3C_2T_x$ MXene at Extreme Temperatures

Ruocun Wang,[1,2,3*] Mark Anayee,[1,2] Yuan Zhang,[1,2] Muhammad Nihal Naseer,[2,4] Teng Zhang,[1,2] Mike Shekhirev,[1,2] Kateryna Shevchuk,[1,2] Yong-Jie Hu,[2] Yury Gogotsi[1,2*]

[1] *A. J. Drexel Nanomaterials Institute, Drexel University, Philadelphia, Pennsylvania 19104, USA*

[2] *Department of Materials Science and Engineering, Drexel University, Philadelphia, Pennsylvania 19104, USA*

[3] *Department of Materials Science and Engineering, University of North Texas, Denton, Texas 76207, USA*

[4] *Centro de Investigación Cooperativa de Energías Alternativas (CIC energiGUNE), Basque Research and Technology Alliance (BRTA), Parque Tecnológico de Álava, Albert Einstein 48, Vitoria-Gasteiz 01510, Spain*

Correspondence should be addressed to Y.G., gogotsi@drexel.edu, and R.W.,

ruocun.wang@unt.edu

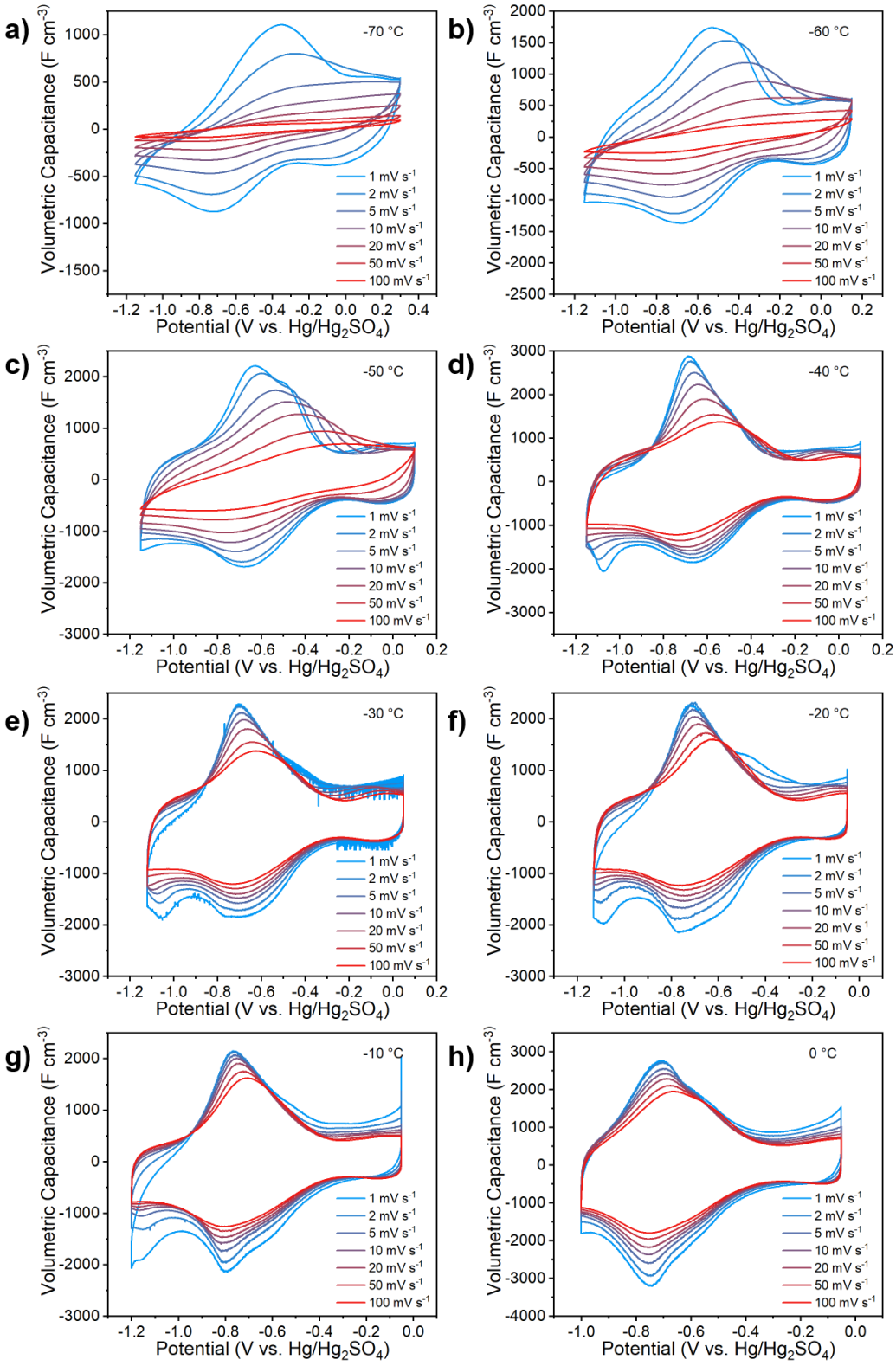

Supplementary Fig. 1 | Cyclic voltammograms of $Ti_3C_2T_x$ MXene in 5 M H_2SO_4 from 1 – 100 mV s^{-1} presented in volumetric capacitance. a–h) represent data collected from -70 to 0 °C, respectively, in 10 °C intervals.

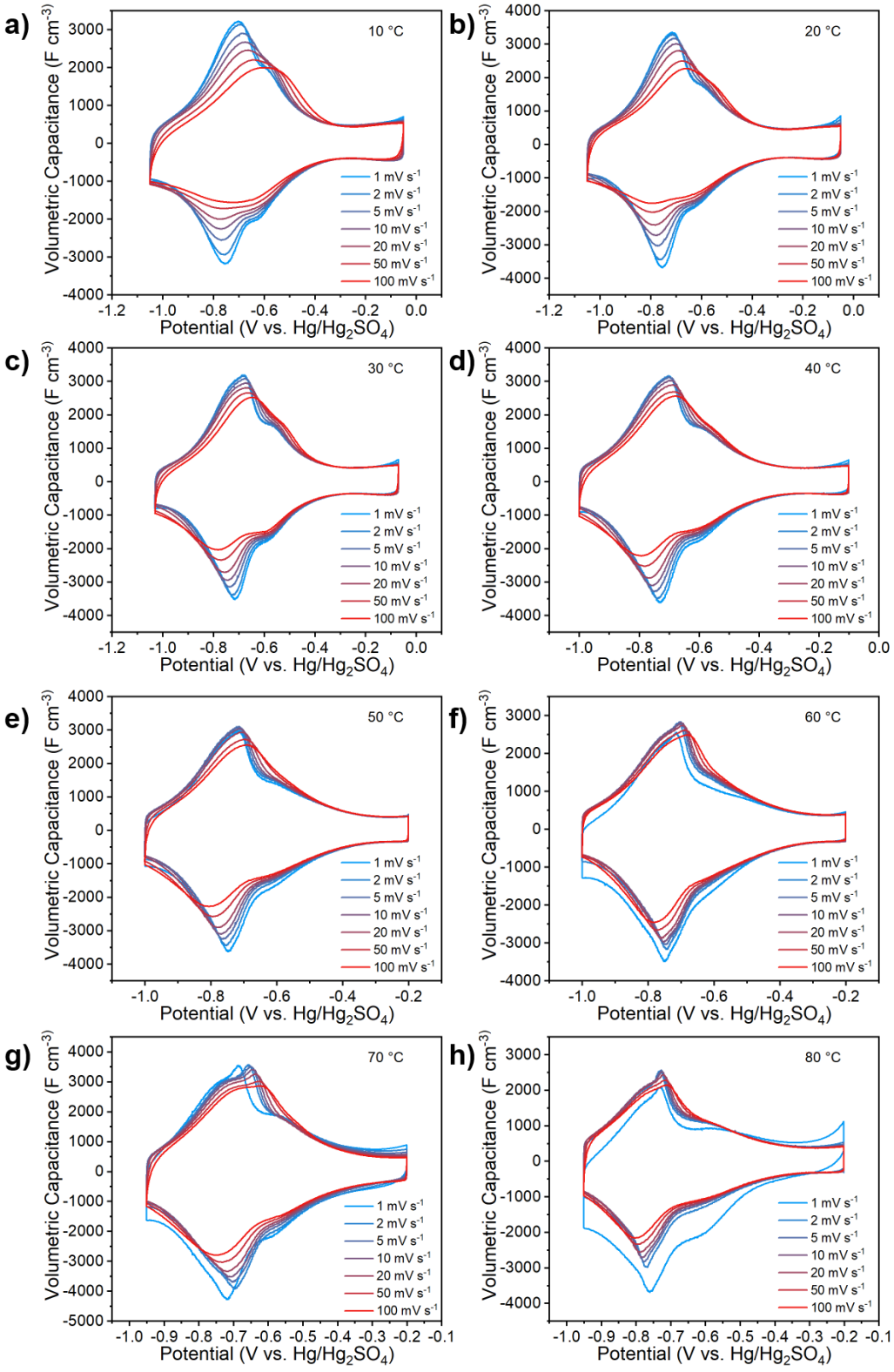

Supplementary Fig. 2 | Cyclic voltammograms of $Ti_3C_2T_x$ MXene in 5 M H_2SO_4 from 1 – 100 mV s^{-1} presented in volumetric capacitance. a–h) represent data collected from 10 to 80 °C, respectively, in 10 °C intervals.

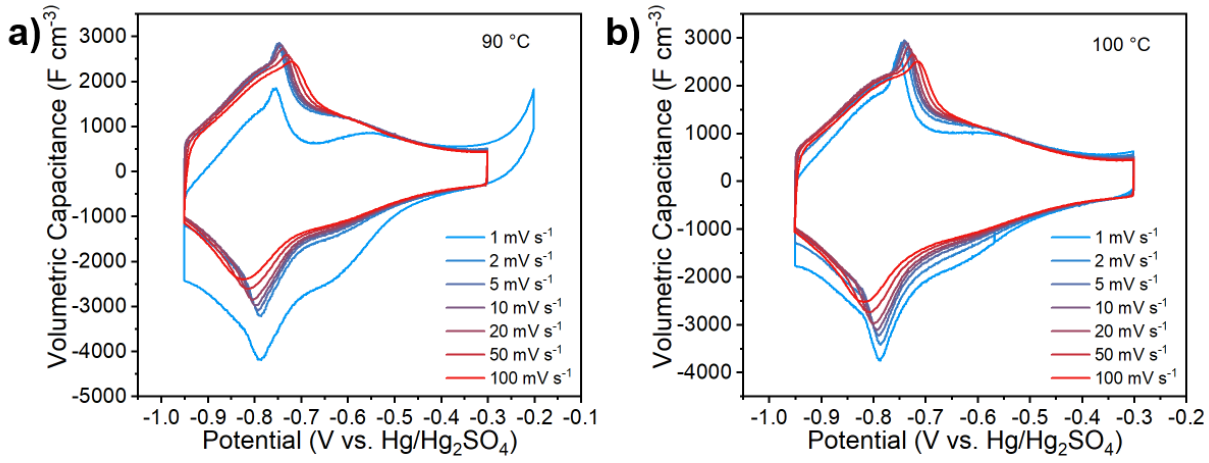

Supplementary Fig. 3 | Cyclic voltammograms of $Ti_3C_2T_x$ MXene in 5 M H_2SO_4 from 1 – 100 mV s^{-1} presented in volumetric capacitance, collected at a) 90 °C and b) 100 °C.

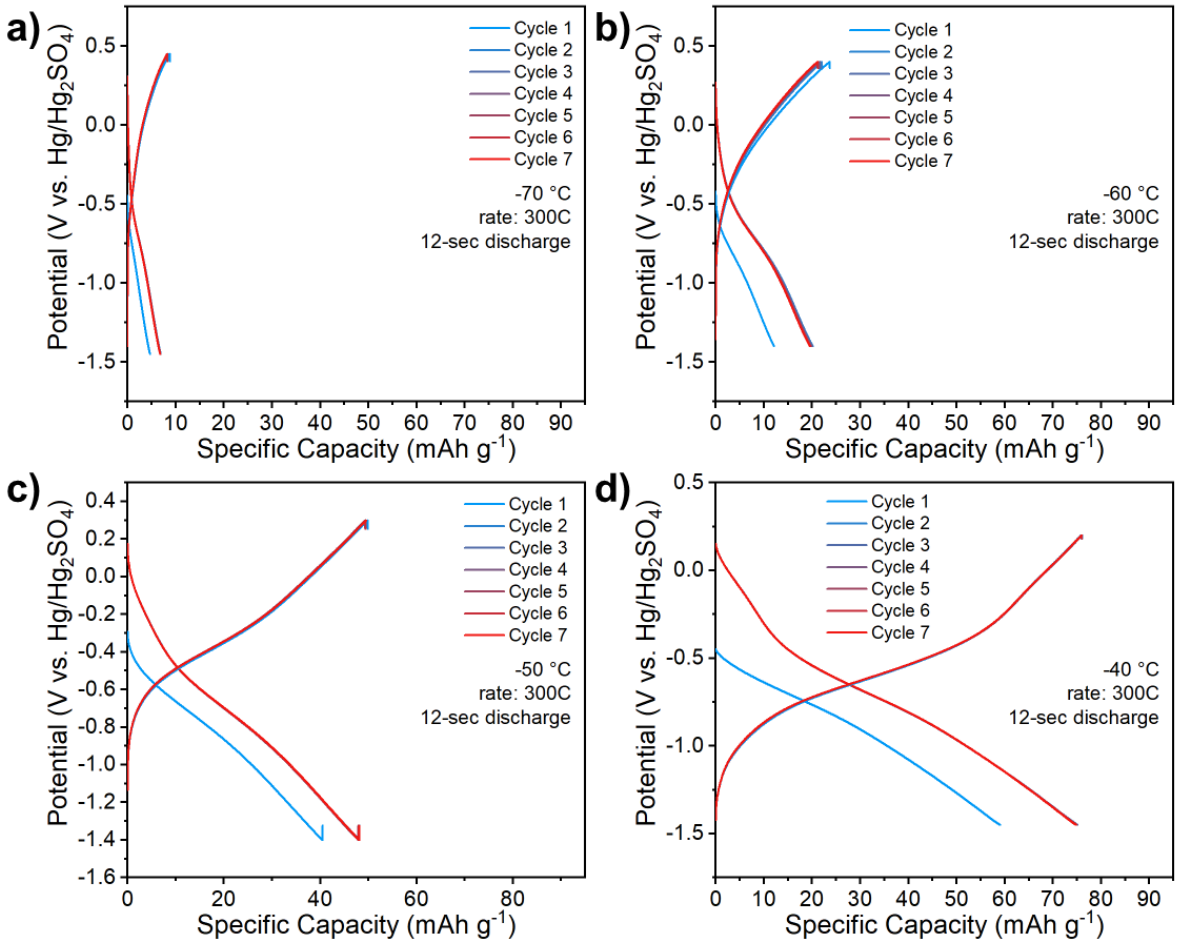

Supplementary Fig. 4 | Galvanostatic charge/discharge curves at a C-rate of 300C (12-sec charge/discharge) of $Ti_3C_2T_x$ MXene in 5 M H_2SO_4, collected at a) -70 °C, b) -60 °C, c) -50 °C, and d) -40 °C.

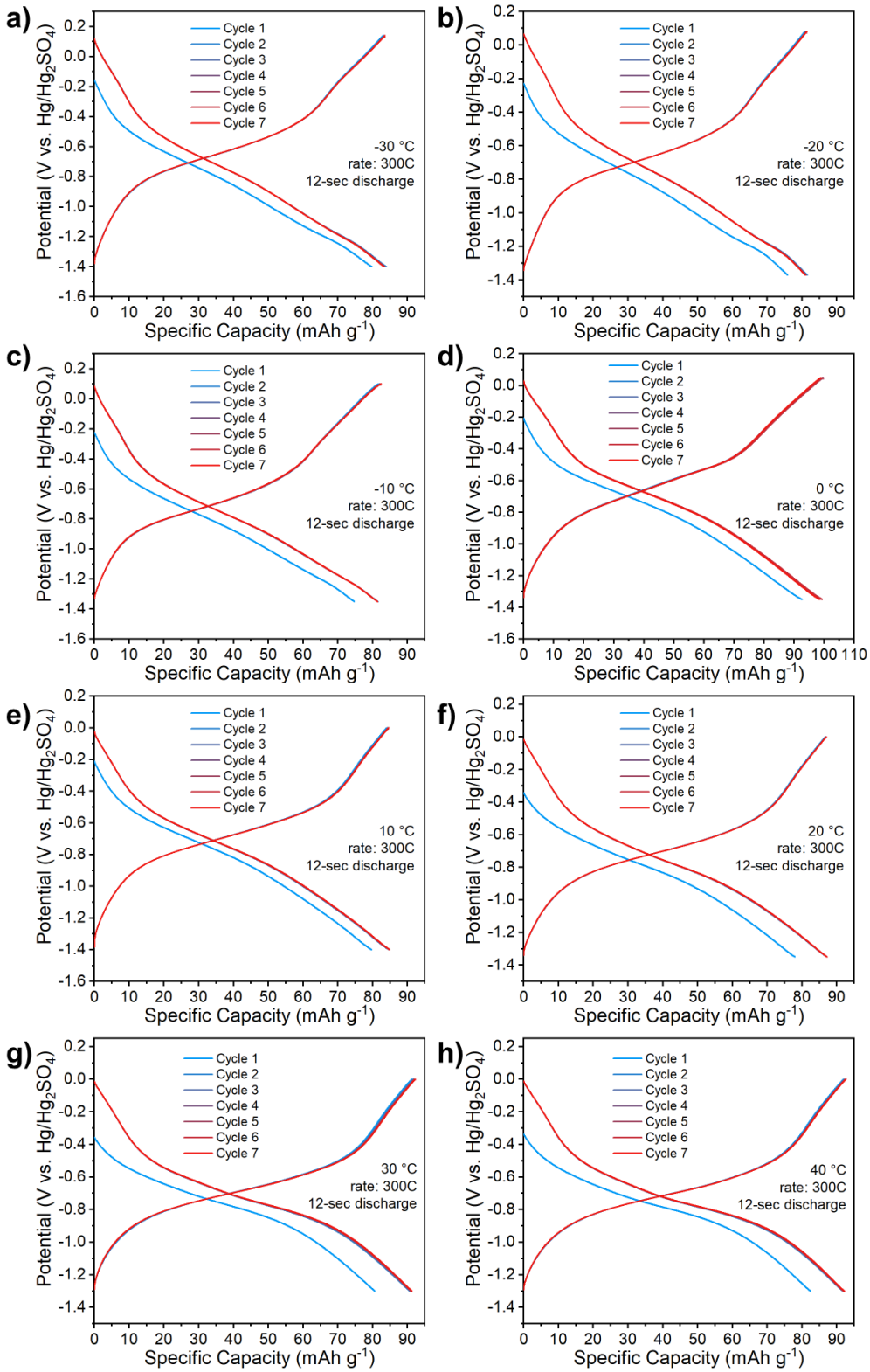

Supplementary Fig. 5 | Galvanostatic charge/discharge curves at a C-rate of 300C (12-sec charge/discharge) of $Ti_3C_2T_x$ MXene in 5 M H_2SO_4. a–h) represent data collected from -30 to 40 °C, respectively, in 10 °C intervals.

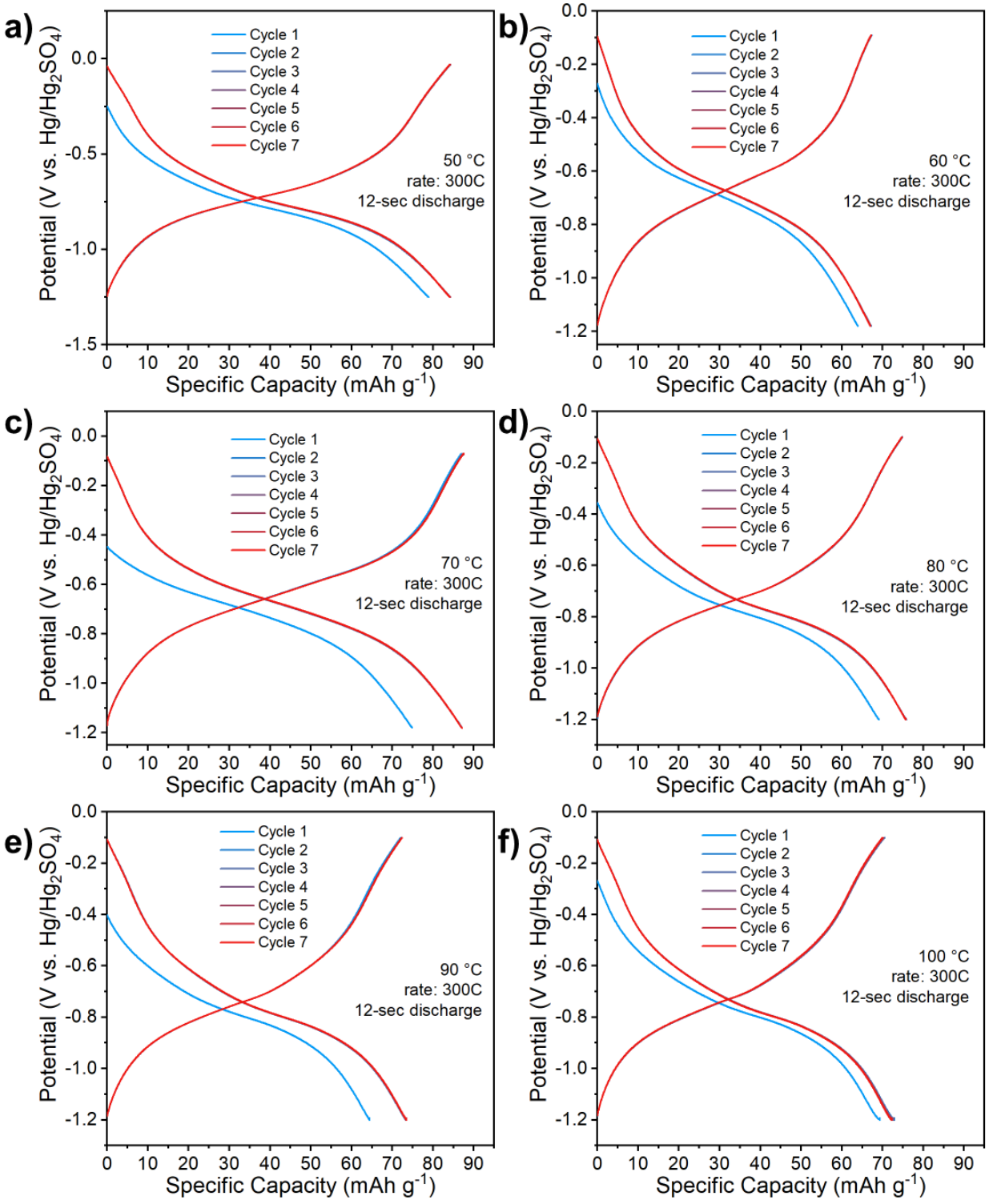

Supplementary Fig. 6 | Galvanostatic charge/discharge curves at a C-rate of 300C (12-sec charge/discharge) of $Ti_3C_2T_x$ MXene in 5 M H_2SO_4. a–f) represent data collected from 50 to 100 °C, respectively, in 10 °C intervals.

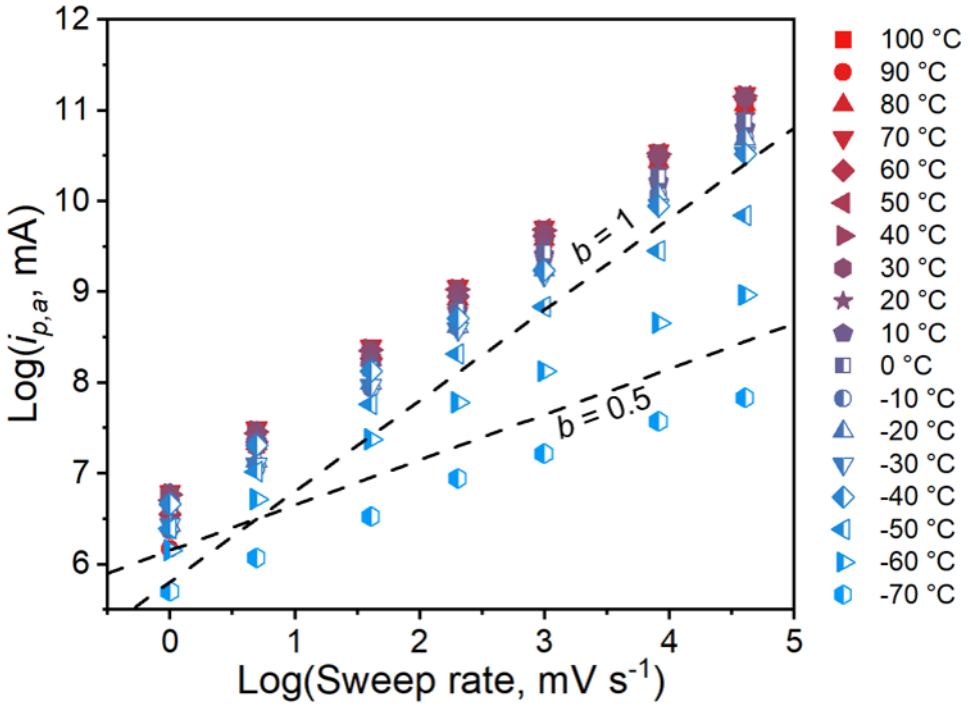

Supplementary Fig. 7 | *b*-value determination from the anodic peak current ($i_{p,a}$) as a function of sweep rate from the cyclic voltammetry data reported in Supplementary Figs. 1–3.

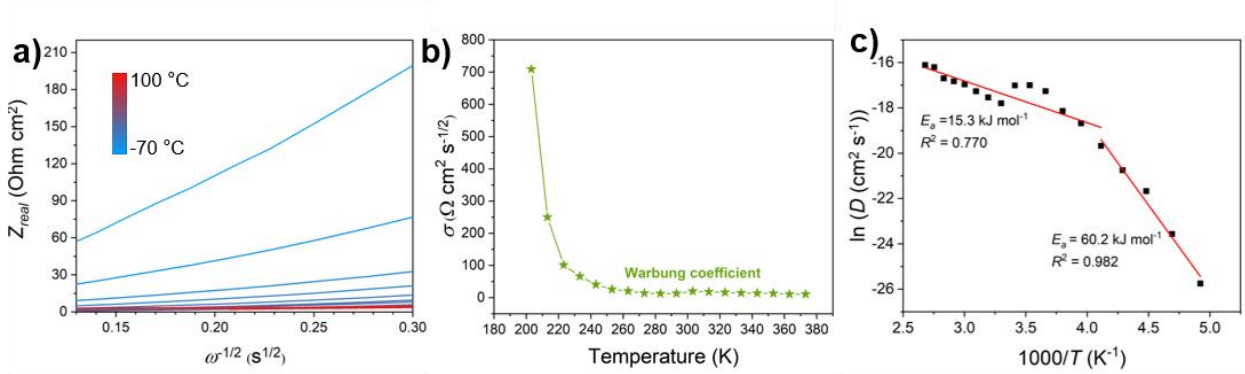

Supplementary Fig. 8 | a) Warburg plot from -70 °C to 100 °C, derived from temperature-dependent electrochemical impedance spectroscopy, b) Warburg coefficient determined from (a) as a function of temperature, and c) activation energy for diffusion obtained from a linear fit between -70 °C and -20 °C, and then between -30 °C and 100 °C.

Supplementary Table 1 | Experimental condition and capacitance retention of carbon-based supercapacitors in aqueous and non-aqueous electrolytes under floating conditions from the literature in comparison to the current work. Abbreviations: PVDF = Polyvinylidene fluoride; PTFE = Polytetrafluoroethylene; TEA = Tetraethylammonium; AN = Acetonitrile; MA = Methyl Acetate; Et_4N = Tetraethylammonium; EiPS = Ethyl isopropyl sulfone.

Category	Label	Material	Electrolyte	Conditions	Length	Retention	Ref
		$Ti_3C_2T_x$ MXene	*5 M H_2SO_4*	*-0.9 V at 70 °C*	*744 h*	*91%*	*This Work*
Aqueous Electrolytes (aq)	1	activated carbon	1 M Li_2SO_4	1.6 V at 25 °C	120 h	93%	[1]
	2	activated carbon	1 M Li_2SO_4	1.7 V at 25 °C	120 h	38%	[1]
	3	carbon cloth	1 M KI / 0.5 M K_2SO_4	1.5 V at 25 °C	120 h	82%	[2]
	4	activated carbon-PVDF	1 M $NaNO_3$	1.6 V at 25 °C	120 h	23%	[3]
	5	activated carbon-PTFE	1 M $NaNO_3$	1.6 V at 25 °C	120 h	90%	[3]
Non-aqueous Electrolytes (non-aq)	1	activated carbon	1 M $TEABF_4$ in AN:MA (75:25)	2.5 V at 60 °C	720 h	92%	[4]
	2	activated carbon	1 M $TEABF_4$ in AN:MA (75:25)	2.7 V at 60 °C	720 h	92%	[4]
	3	activated carbon	1 M $TEABF_4$ in AN	2.5 V at 70 °C	1600 h	81%	[5]
	4	activated carbon	1 M $TEABF_4$ in AN	3.0 V at 70 °C	200 h	59%	[5]
	5	activated carbon	1 M $TEABF_4$ in EiPS	3.4 V at 60 °C	500 h	68%	[6]
	6	activated carbon	1 M $TEABF_4$ in EiPS	3.2 V at 60 °C	500 h	75%	[6]
	7	activated carbon	1 M $TEABF_4$ in EiPS	3.0 V at 80 °C	500 h	63%	[6]
	8	activated carbon	1 M Et_4NBF_4 in AN	3.5 V at 25 °C	500 h	7%	[7]
	9	activated carbon	1 M Et_4NBF_4 in PC	3.5 V at 25 °C	500 h	39%	[7]

Supplementary Note 1 | Calibration of YP-50F activated carbon reference potential against Hg/Hg_2SO_4

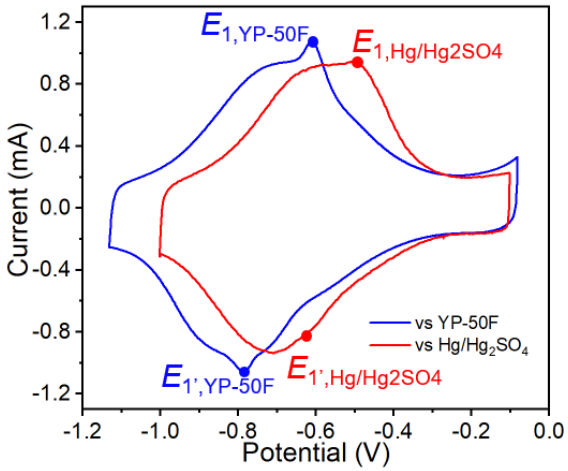

Supplementary Fig. 9 | Cyclic voltammograms of the same $Ti_3C_2T_x$ MXene electrode in 5 M H_2SO_4. The blue curve shows the last cycle in the two-electrode floating test using a YP-50F activated carbon electrode, which serves as both reference and counter electrode. The red curve was recorded in a three-electrode configuration, using a YP-50F activated carbon counter electrode and a reference electrode of Hg/Hg_2SO_4 in saturated K_2SO_4. $E_{1,\text{YP-50F}}$ and $E_{1,\text{Hg/Hg2SO4}}$ represent the same anodic electrochemical process, and $E_{1',\text{YP-50F}}$ and $E_{1',\text{Hg/Hg2SO4}}$ represent the same cathodic electrochemical process.

To convert the YP-50F activated carbon reference potential to the scale *vs.* Hg/Hg_2SO_4, we used the same electrochemical cell used in the two-electrode floating test, added a Hg/Hg_2SO_4 in saturated K_2SO_4 reference electrode, and performed cyclic voltammetry. The voltammograms are compared in **Supplementary Fig. 9**. The standard potential of the electrochemical process 1 (E_1^0) can be calculated by the average potential of the cathodic ($E_{1'}$) and anodic (E_1) processes:

$$E_1^0 = \frac{E_1 + E_{1'}}{2} \tag{S1}$$

In our case,

$$E^0_{1,YP-50F} = \frac{E_{1,YP-50F} + E_{1',YP-50F}}{2} = \text{-0.348 V} \tag{S2}$$

$$E^0_{1,Hg/Hg_2SO_4} = \frac{E_{1,Hg/Hg_2SO_4} + E_{1',Hg/Hg_2SO_4}}{2} = \text{-0.279 V} \tag{S3}$$

Since E_1^0 is the same process but against different reference electrodes, we can convert the potential between the two reference electrodes by taking into account the difference:

$$E\,(vs.\ Hg/Hg_2SO_4) = E\,(vs.\ \text{YP-50F}) - E_{1,\text{YP-50F}}{}^0 + E_{1,\text{Hg/Hg2SO4}}{}^0 = E\,(vs.\ \text{YP-50F}) + 0.069\ \text{V} \tag{S4}$$

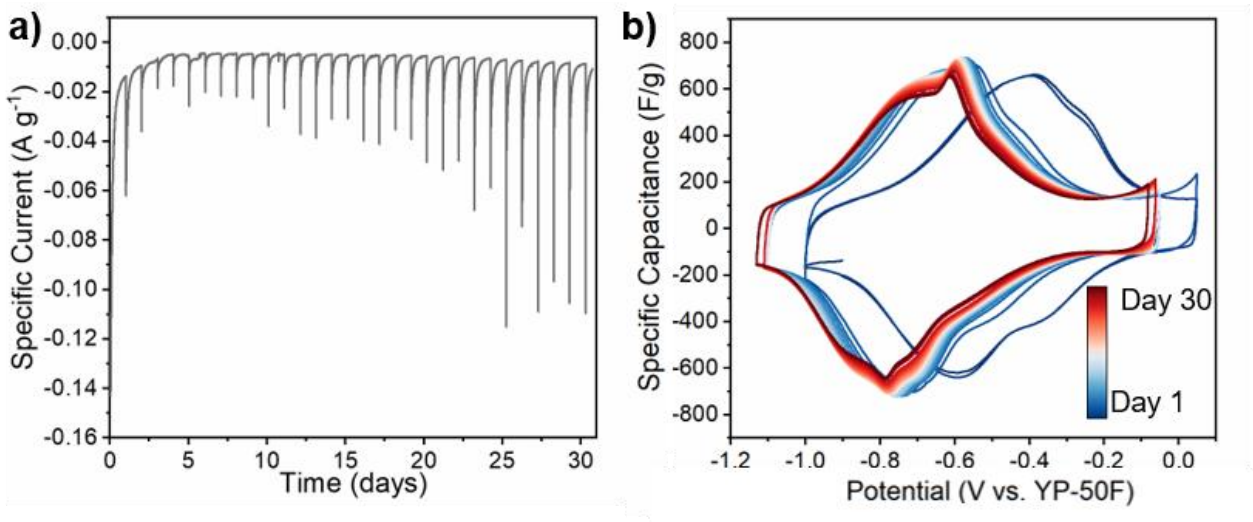

Supplementary Fig. 10 | Current profile of $Ti_3C_2T_x$ MXene in 5 M H_2SO_4 during the 30-day floating at a potential of -0.9 V *vs.* YP-50F and the cyclic voltammograms at 20 mV s^{-1} performed at the end of each day for capacitance measurement.

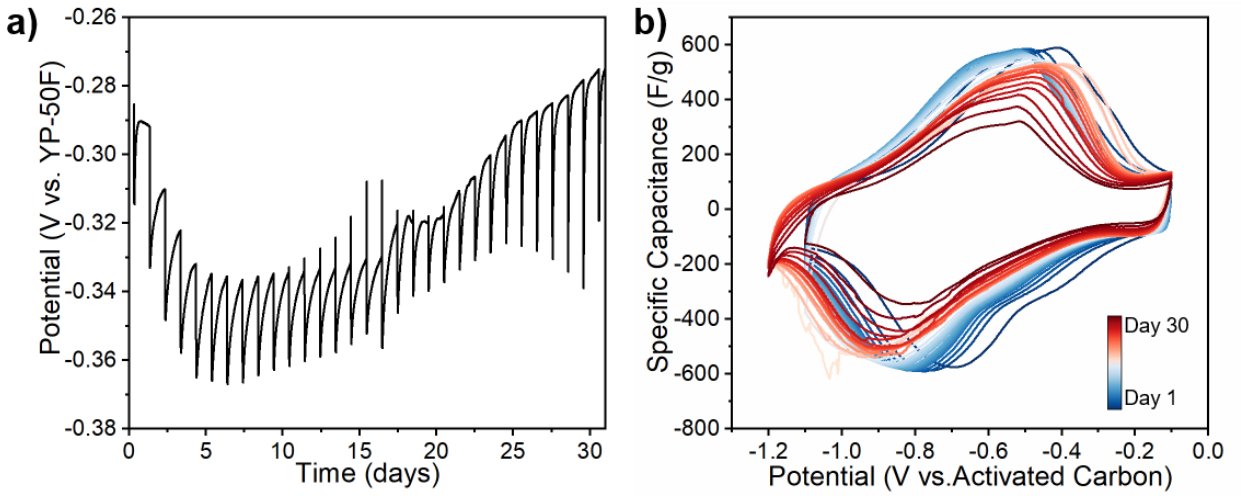

Supplementary Fig. 11 | Potential profile of $Ti_3C_2T_x$ MXene in 5 M H_2SO_4 during 30 days at open-circuit potential and the cyclic voltammograms at 20 mV s^{-1} performed at the end of each day for capacitance measurement. Activated carbon is YP-50F.

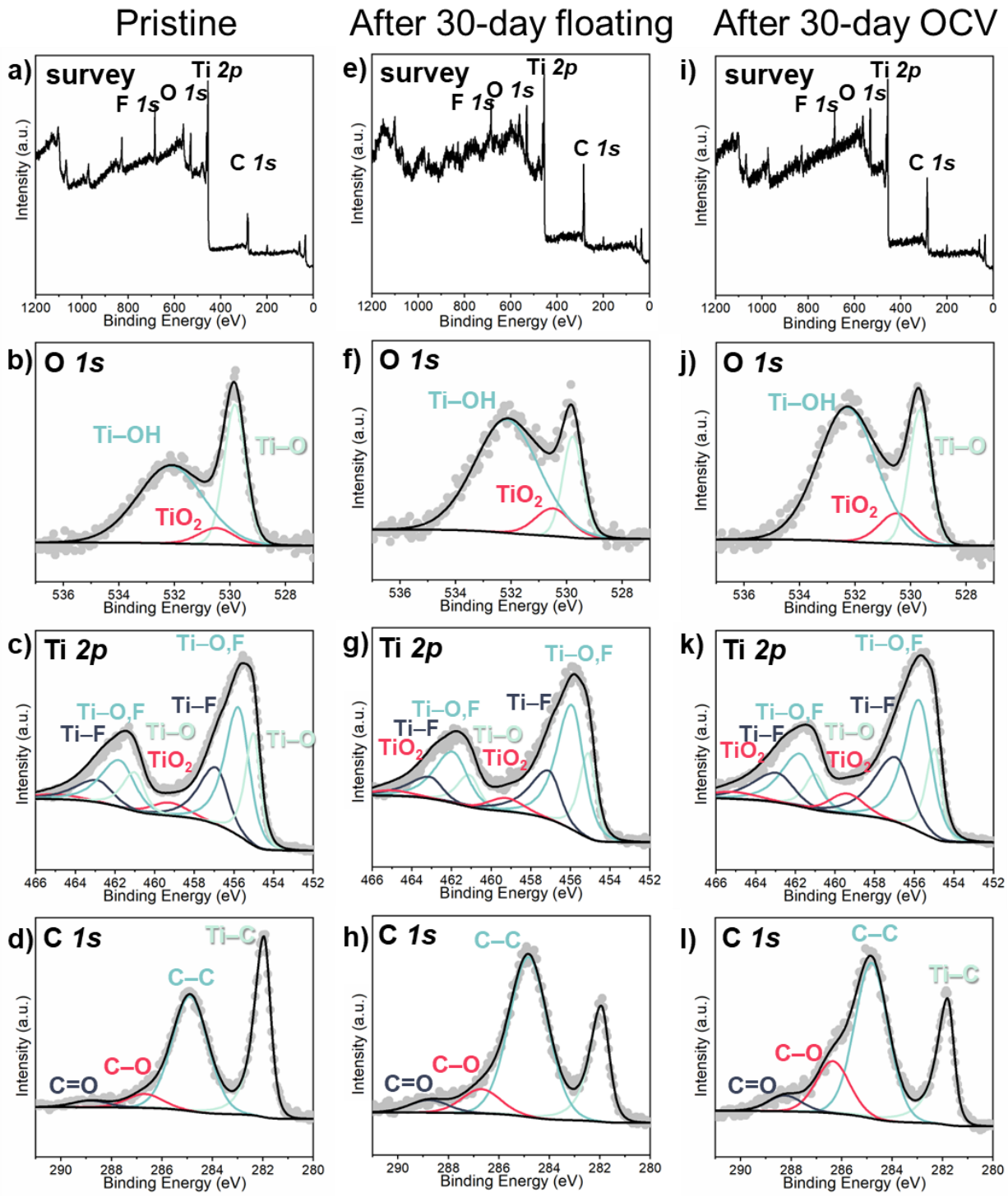

Supplementary Fig. 12 | XPS spectra of $Ti_3C_2T_x$ thin film electrodes before and after aging in electrochemical cells. We show the survey scan, the high-resolution scans of O 1*s*, Ti 2*p*, and C 1*s* regions, respectively, for a-d) pristine $Ti_3C_2T_x$, e-h) $Ti_3C_2T_x$ after 30-day floating at -0.9 V *vs.* YP-50F in 5 M H_2SO_4, i-l) $Ti_3C_2T_x$ after 30 days at open-circuit potential in 5 M H_2SO_4.

Supplementary Table 2 | Elemental analysis of supernatant solutions collected from filtered $Ti_3C_2T_x$ MXene suspensions in 5 M H_2SO_4 and DI water after aging, measured using inductively coupled plasma optical emission spectroscopy (ICP-OES). The ppm unit in the table represents mg L^{-1}. Sc and Y are included as internal standards.

Sample Name	Li 670.783 nm	Ti 334.941 nm	Sc 361.383 nm	Y 377.433 nm
Solution from 0.5 g L^{-1} $Ti_3C_2T_x$ in 5 M H_2SO_4 for 491 days	2.9 ppm	214.1 ppm	0.98 (ratio)	0.97 (ratio)
Solution from 0.5 g L^{-1} $Ti_3C_2T_x$ in DI water for 491 days	2.5 ppm	0 ppm	1.02 (ratio)	1.02 (ratio)
Solution from the 5 M H_2SO_4 electrolyte used in the two-electrode electrochemical cell of $Ti_3C_2T_x$ at open-circuit condition and 70 °C for 1 month	0.00 ppm	60 ppm	1.03 (ratio)	1.03 (ratio)

Supplementary Note 2 | Calculating the extent of titanium dissolution based on ICP-OES data

ICP-OES results allow us to measure the extent of Ti dissolution after the aging experiments. To compare the ICP-OES results in **Supplementary Table 2** with the initial MXene content, we calculated the number of moles and molar concentrations of soluble Ti species using equations S5–S7 and reported the results in **Supplementary Table 3**.

The number of moles of soluble Ti species, n_{Ti}, in a solid MXene can be calculated by equation S5:

$$n_{Ti} = \frac{3 \times m_{Ti_3C_2T_x}}{MTi_3C_2T_x} \quad \text{(S5)}$$

where, $m_{Ti3C2Tx}$ is the mass of $Ti_3C_2T_x$ and $M_{Ti3C2Tx}$ is the molar mass of $Ti_3C_2T_x$. Assuming the formula unit of $Ti_3C_2O_{0.300}OH_{0.614}F_{1.016}Cl_{0.070}$,[8] we have a molar mass of 204.65 g mol^{-1}.

The number of moles of soluble Ti species, n_{Ti}, in the supernatant of MXene solution measured by ICP-OES can be calculated by equation S6:

$$n_{Ti} = \frac{m_{Ti}}{M_{Ti}} \quad \text{(S6)}$$

where, m_{Ti} is the mass of Ti and M_{Ti} is the molar mass of Ti, 47.867 g mol^{-1}.

The molar concentration of soluble Ti species, C_{Ti}, can be calculated using equation S7:

$$C_{Ti} = \frac{n_{Ti}}{V} \quad \text{(S7)}$$

where, V is the volume of the solution. In the electrochemical cell, the total volume of the electrolyte, 5 M H_2SO_4, was about 450 µL, and the mass of the $Ti_3C_2T_x$ electrode was 88.3 µg.

The percentage of Ti dissolution can be calculated by the ratio of the C_{Ti} measured by ICP-OES and the initial C_{Ti} in the system.

$$Ti_{dissolution}\% = \frac{C_{Ti,inital}}{C_{Ti,final}} \quad \text{(S8)}$$

The amount of $Ti_3C_2T_x$ electrode that remained after the 30-day OCV at 70 °C was calculated by

$$n_{Ti,final} = n_{Ti,initial} \times (1 - Ti_{dissolution}\%) \quad \text{(S9)}$$

where, $n_{Ti,\ initial}$ is the number of moles of soluble Ti species in the pristine electrode before the electrochemical test. The molar concentration results are presented in **Supplementary Table 3.**

Supplementary Table 3 | Molar concentrations of soluble Ti species in the system and supernatant solutions collected from filtered $Ti_3C_2T_x$ MXene suspensions in 5 M H_2SO_4 and DI water after aging, measured using inductively coupled plasma optical emission spectroscopy (ICP-OES).

Sample Name	Initial C_{Ti} in the system	Final C_{Ti} in the supernatant	Percentage of Ti Dissolution
Solution from 0.5 g L^{-1} $Ti_3C_2T_x$ in 5 M H_2SO_4 for 491 days	7.33 mmol L^{-1}	4.18 mmol L^{-1}	57%
Solution from 0.5 g L^{-1} $Ti_3C_2T_x$ in DI water for 491 days	7.33 mmol L^{-1}	0 ppm	0%
Solution from the 5 M H_2SO_4 electrolyte used in the two-electrode electrochemical cell of $Ti_3C_2T_x$ at open-circuit condition and 70 °C for 1 month	2.88 mmol L^{-1}	1.25 mmol L^{-1}	44%

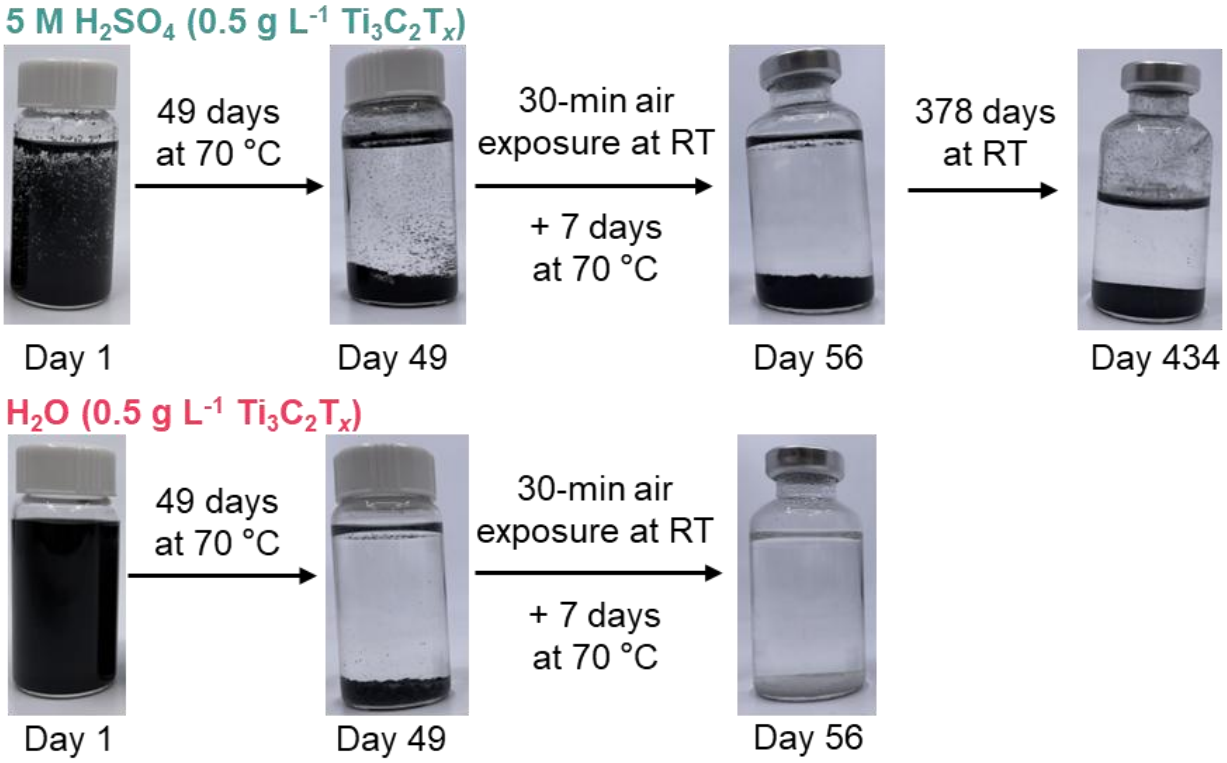

Supplementary Fig. 13 | Digital photographs of 0.5 g L^{-1} $Ti_3C_2T_x$ MXene suspension in 5 M H_2SO_4 and DI water taken as a function of time. The storage temperature, duration, and action in between the times of the pictures taken were labeled next to the arrow signs.

Supplementary Table 4 | Potential windows used in cyclic voltammetry and galvanostatic charge/discharge tests and the current density used in galvanostatic charge/discharge tests at different temperatures.

Temperature	Cyclic Voltammetry	Galvanostatic charge/discharge @300C	
°C	Potential window [V vs. Hg/Hg_2SO_4]	Potential window [V vs. Hg/Hg_2SO_4]	Current density [A/g]
-70	-1.15 – 0.30	-1.45 – 0.45	2.30
-60	-1.15 – 0.30	-1.40 – 0.40	6.37
-50	-1.15 – 0.10	-1.40 – 0.30	14.44
-40	-1.15 – 0.10	-1.45 – 0.20	27.48
-30	-1.12 – 0.05	-1.40 – 0.14	24.63
-20	-1.13 – -0.05	-1.37 – 0.08	24.22
-10	-1.02 – -0.05	-1.35 – 0.10	24.26
0	-1.00 – -0.05	-1.35 – 0.05	30.00
10	-1.05 – -0.05	-1.40 – 0.00	25.28
20	-1.05 – -0.05	-1.35 – 0.00	25.95
30	-1.03 – -0.07	-1.30 – 0.00	27.18
40	-1.00 – -0.10	-1.30 – 0.00	27.37
50	-1.00 – -0.20	-1.25 – -0.03	25.08
60	-1.00 – -0.20	-1.18 – -0.09	20.10
70	-0.95 – -0.20	-1.18 – -0.07	26.14
80	-0.95 – -0.20	-1.20 – -0.10	22.37
90	-0.95 – -0.30	-1.20 – -0.10	21.45
100	-0.95 – -0.30	-1.20 – -0.10	21.45

References

1. Ratajczak P, Jurewicz K, Skowron P, Abbas Q, Béguin F (2014) Effect of accelerated ageing on the performance of high voltage carbon/carbon electrochemical capacitors in salt aqueous electrolyte. Electrochimica Acta 130:344–350. https://doi.org/10.1016/j.electacta.2014.02.140

2. Platek A, Piwek J, Fic K, Frackowiak E (2019) Ageing mechanisms in electrochemical capacitors with aqueous redox-active electrolytes. Electrochimica Acta 311:211–220. https://doi.org/10.1016/j.electacta.2019.04.117

3. Abbas Q, Pajak D, Frąckowiak E, Béguin F (2014) Effect of binder on the performance of carbon/carbon symmetric capacitors in salt aqueous electrolyte. Electrochimica Acta 140:132–138. https://doi.org/10.1016/j.electacta.2014.04.096

4. Iwama E, Taberna PL, Azais P, Brégeon L, Simon P (2012) Characterization of commercial supercapacitors for low temperature applications. Journal of Power Sources 219:235–239. https://doi.org/10.1016/j.jpowsour.2012.07.029

5. Kötz R, Ruch PW, Cericola D (2010) Aging and failure mode of electrochemical double layer capacitors during accelerated constant load tests. Journal of Power Sources 195:923–928. https://doi.org/10.1016/j.jpowsour.2009.08.045

6. Köps L, Kreth FA, Leistenschneider D, Schutjajew K, Gläßner R, Oschatz M, Balducci A (2022) Improving the Stability of Supercapacitors at High Voltages and High Temperatures by the Implementation of Ethyl Isopropyl Sulfone as Electrolyte Solvent. Advanced Energy Materials 2203821. https://doi.org/10.1002/aenm.202203821

7. Ruch PW, Cericola D, Foelske A, Kötz R, Wokaun A (2010) A comparison of the aging of electrochemical double layer capacitors with acetonitrile and propylene carbonate-based electrolytes at elevated voltages. Electrochimica Acta 55:2352–2357. https://doi.org/10.1016/j.electacta.2009.11.098

8. Michałowski PP, Anayee M, Mathis TS, Kozdra S, Wójcik A, Hantanasirisakul K, Jóźwik I, Piątkowska A, Możdżonek M, Malinowska A, Diduszko R, Wierzbicka E, Gogotsi Y (2022) Oxycarbide MXenes and MAX phases identification using monoatomic layer-by-layer analysis with ultralow-energy secondary-ion mass spectrometry. Nature Nanotechnology 17:1192–1197. https://doi.org/10.1038/s41565-022-01214-0